Topological and metric properties of Hénon-type strange attractors

Predrag Cvitanović
Niels Bohr Institute, Blegdamsvej 17, DK-2100 Copenhagen, Denmark

Gemunu H. Gunaratne
The James Franck Institute, University of Chicago, Chicago, Illinois 60637

Itamar Procaccia
The James Franck Institute, University of Chicago, Chicago, Illinois 60637
and Department of Chemical Physics, Weizmann Institute of Science, Rehovot 76100, Israel
(Received 23 November 1987)

We use the set of all periodic points of Hénon-type mappings to develop a theory of the topological and metric properties of their attractors. The topology of a Hénon-type attractor is conveniently represented by a two-dimensional symbol plane, with the allowed and disallowed orbits cleanly separated by the "pruning front." The pruning front is a function discontinuous on every binary rational number, but for maps with finite dissipation $|b|<1$, it is well approximated by a few steps, or, in the symbolic dynamics language, by a finite grammar. Thus equipped with the complete list of allowed periodic points, we reconstruct (to resolution of order b^n) the physical attractor by piecing together the linearized neighborhoods of all periodic points of cycle length n. We use this representation to compute the singularity spectrum $f(\alpha)$. The description in terms of periodic points works very well in the "hyperbolic phase," for α larger than some α_c, where α_c is the value of α corresponding to the (conjectured) phase transition.

I. INTRODUCTION

The aim of this paper is a quantitative understanding of strange attractors of Hénon type. The Hénon mapping[1] is given by

$$x'=y+a-x^2\ ,$$
$$y'=bx\ . \tag{1.1}$$

Hénon has conjectured that for $a=1.4$ and $b=0.3$ the limit cycle of this mapping is a strange attractor. This attractor[1] is the prototypical strange attractor,[2] and Hénon's enlargements of it are some of the most frequently reproduced figures in reviews of topics in the field of nonlinear dynamics.[3,4] Understanding of the Hénon-type strange attractors is a central problem of nonlinear dynamics because such attractors are believed to be generic for low-dimensional dynamical systems observed either experimentally or modeled by equations such as the Lorenz equations.[5]

To the naked eye, the Hénon attractor looks locally self-similar. It is our goal here to construct a scheme which encodes this self-similarity, and yields both a qualitative and a quantitative description of such strange sets. By the qualitative understanding of the attractor we mean the complete enumeration of all possible motions; quantitative understanding requires also inclusion of the length scales associated with a particular physical realization.

Our strategy is the following: we first construct a two-dimensional representation of the symbolic dynamics of the map. This is a "road map" in which the various sheets of the stable and unstable manifolds are represented by straight sections, and the topology is preserved: the nearby periodic points in the symbol plane represent nearby periodic points in the physical space. This representation enables us to separate the allowed and the forbidden orbits by means of a "pruning front," a boundary between the two kinds of orbits. The pruning front is a function, which calls for infinite number of parameters for its specification. However, we shall show that this function is discontinuous on a countable number of points (binary rational numbers) and that the size of the discontinuity decreases exponentially for maps with finite dissipation. This will allow us to specify to high precision the allowed orbits with a finite grammar.

The above results specify the symbolic dynamics of any map of Hénon type. The particular physical attractor is then reconstructed by piecing together the linear approximations to the small neighborhoods of periodic points. As we know all allowed orbits and their eigenvalues, we are able to systematically and uniformly cover the attractor, and extract the corresponding thermodynamic functions[6] to unprecedented accuracy.

There are three main ingredients that make the systematic description feasible. The first two are quite general: a strange attractor is densely covered by periodic points, and these points are hierarchically ordered according to the length of the corresponding cycles. The third ingredient is particular to the Hénon-type mappings: the periodic points lie on binary trees.

Intuitively it is clear that a strange attractor should be dense with periodic points: by its definition,[7,2] a strange attractor is ergodic, strongly mixing and connected, so

 ©1988 The American Physical Society

the orbit of any typical point P passes arbitrarily close to P. But if the trajectory returns close to the starting point after n iterations, generally one can gently readjust the starting point in such a way that the orbit exactly returns to it after n iterations. Conversely, if we know the location and the stability of a periodic point, we also know the structure of the strange attractor in its neighborhood.

The next important insight is the realization that the cycle points naturally separate into a hierarchy whose nth level consists of all the cycles of length n. Consider how a strange attractor unfolds itself if we iterate its basin of attraction (cf. Fig. 1). If the process is stopped after one iteration, we have the coarsest outline of the attractor. The thickness will be an indication of the contraction rate of the mapping, and if it has a fixed point, this thickness will roughly be the contracting eigenvalue at that fixed point. After two iterations, the attractor contracts further but also folds upon itself. The thickness of the strips will be of the order of the square of the fixed point eigenvalue and of the contracting eigenvalues of the period-2 cycles which live on these strips. After n time steps, the attractor takes a shape that contains all the n cycles, and its local scale will be characterized by the eigenvalue of the neighboring n cycle. So what is experimentally attainable is a hierarchy of scales, finer scales corresponding to longer cycles, and this is precisely the hierarchy which will be the basis for our metric description of the strange attractor.[8–10]

This description of a strange attractor is analogous to the description of real numbers in terms of the rational numbers. The periodic orbits correspond to rational numbers, and aperiodic orbits (trajectories that wander ergodically across the attractor) to irrational numbers. To any finite resolution, one can bracket an ergodic orbit by nearby periodic points, and even though the periodic points are a set of measure zero, they provide a good description of all points on the attractor. In particular, since locally the map can be approximated by a linear transformation, the local structure of the attractor can be deduced from the Jacobian of the (n times iterated) map at the periodic point. Thus, if the periodic points are dense on the attractor, the entire attractor can be described by this scheme, and a variety of experimentally relevant numbers can be extracted. As an example, we shall evaluate the generalized dimensions and the singularity spectra of the Lozi[11] and the Hénon attractors.

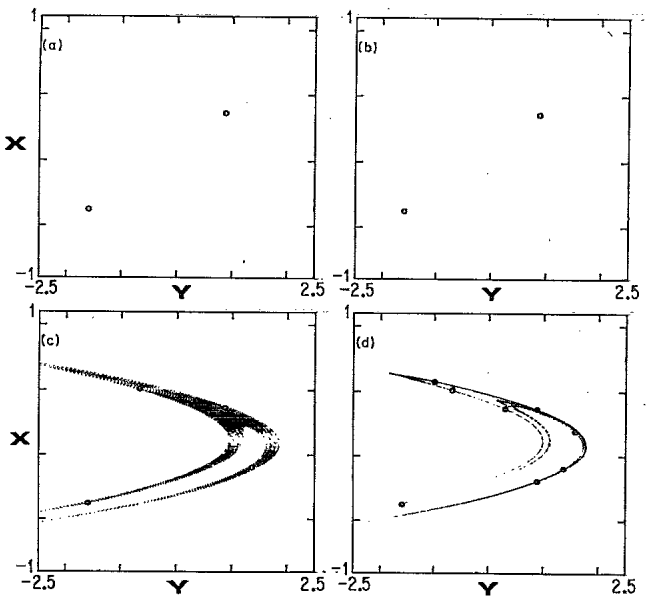

FIG. 1. Successive iterations of the plane by the Hénon map $(x,y)\to(y+a-x^2,bx)$ with $a=1.4, b=0.3$. The circles are the periodic points of increasing order.

The next ingredient, the binary structure, is particular to the Hénon-type mappings. A small segment of a strange attractor is stretched by iteration; since the attractor is contained within a finite region of space, it must fold. A Hénon-type attractor folds the plane back into itself exactly once, and this is the reason why a binary structure[12,13] can describe orbits on it. Other dynamical systems, like maps of the annulus in their supercritical regime,[14,15] will not be describable by binary trees, since the mapping folds phase space more than once. An analogous theory with ternary trees was shown recently[15] to lead to a similar understanding of the strange attractors of those systems as well.

However, even though every allowed orbit has a unique binary label, the binary tree is not complete; disallowed orbits are "pruned" from it. Finding the rules for pruning is one central result in this paper, see Sec. II D. As is already clear from the study of one-dimensional (1D) maps, the form of the attractor varies with the parameter in a very complex fashion. In this paper we concentrate not on the attractor itself, but on the smoothly varying envelope of the attractor,[16] which is the union of all periodic orbits of the map. Its closure always includes the attractor, but is, in general, larger than the attractor. As the parameters are varied, the attractor varies wildly: it collapses to periodic orbits, develops small chaotic bands, blows up at the crisis points. All the while the set of periodic orbits, deforms gently, and as the attractor goes through its extravagant gyrations, its outline vanishes and reappears.

The genesis of the visible attractor can be visualized as a random walk on the union of all periodic points. A physical trajectory is squeezed onto a nearby periodic point by its contracting eigenvalue, and is thrown out along the unstable direction, where it again lands close to some other periodic point. If it reaches a stable orbit, the trajectory remains in it forever; otherwise it continues its wandering across the union of all periodic points, tracing out a strange attractor. Whether one can go from periodic point A to the periodic point B depends on whether the unstable manifold of A intersects the stable manifold of B: this defines a flow diagram on the union of all periodic points, dividing it into a transient part, and the asymptotically visible strange attractor.[17] In practice, the periodic orbits which belong to the visible attractor can be extracted from a chaotic time series.[8]

In Sec. II we review the symbolic dynamics of unimodal maps in one dimension,[18–20] and extend it to maps of the plane of the Hénon type. The iteration of a point by the Hénon map is equivalent to the application of an area preserving transformation on a symbolic plane. The sym-

bol plane is used to understand how to construct binary trees with finite grammar that knocks off disallowed branches to yield topological descriptions of the underlying attractors. Explicit calculations are presented for the Lozi map, and for the Hénon map.

As we shall see, the binary tree that describes the topology of the periodic orbits is not a complete tree. The number of legs at its nth level grows slower than 2^n. In fact its rate of growth is an estimate to topological entropy K_0 of the map. This number can be calculated as

$$K_0 = \lim_{n\to\infty} \frac{1}{n} \ln N_n \ , \tag{1.2}$$

where N_n is the number of points belonging to periodic orbits of length n.

We shall argue that the elucidation of the symbolic representation of the periodic orbits and their organization on a tree equipped with a local grammar allows systematic computations of the topological entropy. One major result is that different maps have the same topological entropy at analogous points of their parameter space (to be defined below), and explicit calculations can be done, at least to first order in a smallness parameter which is the inverse of the dissipation.

In Sec. III we turn to the metric properties. The scaling descriptions of the invariant measure in terms of the spectrum of scaling indices[6] (or singularities) is reviewed; the relations between the local Jacobians and the scaling exponents[9,10,15] are used to calculate the scaling exponents and their rate of occurrence on the set [the $f(\alpha)$ function]. Section IV offers a summary and conclusions. In particular we discuss how the ideas developed in this paper may be useful in the development of an ergodic theory for chaotic systems.

II. TOPOLOGY OF HÉNON-TYPE MAPS

A. Symbolic dynamics of unimodal maps in one dimension

The simplest maps that stretch the domain D and fold it are unimodal maps on the interval. The domain is partitioned in two at the (unique) turning point C (which without loss of generality is assumed to be 0), and points on the right of C are denoted by 1 (or R), and those on its left are denoted by 0 (or L). For a unimodal map f

$$\begin{aligned} f'(x) &\geq 0 \quad \text{if } x<0 \\ f'(x) &\leq 0 \quad \text{if } x>0 \ . \end{aligned} \tag{2.1}$$

With any point $x\in D$ associate a sequence of symbols $\{a_k\}$ where

$$a_k = \begin{cases} 1 & \text{if } f^{(k-1)}(x)\geq 0 \\ 0 & \text{otherwise} \ . \end{cases} \tag{2.2}$$

Here $f^{(m)}$ denotes m compositions of the map, $f^{(0)}(x)=x$. The sequence $\{a_k\}$ is called the itinerary of x and represents its "symbolic future." (The future in this definition includes the present.) Observe that the itinerary of $f^{(m)}(x)$ is $\{a_{k+m}\}$. The order (along the x axis) of two points x and y can be determined from the corresponding itineraries by converting their symbol sequences into binary numbers. Because of the continuous refolding of the interval, the corresponding binary number is not $a_1a_2a_3$, but the number given by the alternating binary tree (see Fig. 2). Algebraically the alternating binary label is given by

$$\gamma = 0.c_1c_2\ldots = \sum_{k=1}^{\infty} c_k 2^{-k} \ , \tag{2.3}$$

where

$$c_k = \sum_{i=1}^{k} a_i \ (\text{mod}2) \tag{2.4}$$

(this is discussed in more detail in the Appendix A). Thus the ordering of points on D is determined by its symbolic future (i.e., the itinerary), the immediate future being the most significant. For the tent map

$$T(x) = 1-2\,|x\,| \tag{2.5}$$

the point with a given itinerary is exactly evaluated from (2.3), apart from a linear transformation.

B. Symbol plane

In this section we generalize the 1D ordering of Sec. II A to a 2D symbol plane. The relative ordering of points in the symbol plane reflects the relative ordering of the corresponding points in the physical space. As mentioned before, forward iterations of Hénon-type mappings produce an increasing number of folds. The fold to which a point belongs is determined by its symbolic history. Backward iterations of the map produce the stable manifold folds, (generally) transverse to the forward folds, so location along the fold is determined by the symbolic future. The relation of the physical attractor to the corresponding symbol plane is illustrated in Figs. 1, 3, and 4. Use of the symbol plane simplifies considerably the description of the union of all periodic points. Instead of looking directly at the physical stable and unstable manifolds of a particular Hénon-type map, we study a straight-grid representation of the symbolic dynamics which preserves the topology of the set and which is at the same time common to an entire class of Hénon-type maps.

Define a sequence $\{d_k\}$ and a number δ analogous to $\{c_k\}$ and γ of Sec. II A. Just as γ gave the ordering of points on the axis of unimodal maps, δ will give the ordering of points transversely on a Hénon-type attractor. The pair of points (γ,δ) will then specify the coarse-grained position of a point on the attractor. The results developed in this section are valid for (1.1) with $b>0$.

Let $f:D\to D$ be a unimodal map [Fig. 3(a)] defined onto the interval D [e.g., $f(x)=2-x^2$]. Without loss of generality we assume that $D=[-1,1]$ and that the critical point C is at 0. Consider the action of f on D. An iteration will stretch D by a factor of 2 and fold it once as shown in Fig. 1(c). For Hénon-type maps with $b>0$ the folding is qualitatively the same. To see this we only need to note that from the second equation of (1.1), those points with $x<0$ are mapped to the half-plane $y<0$. Thus after an iteration D was folded in such a way that

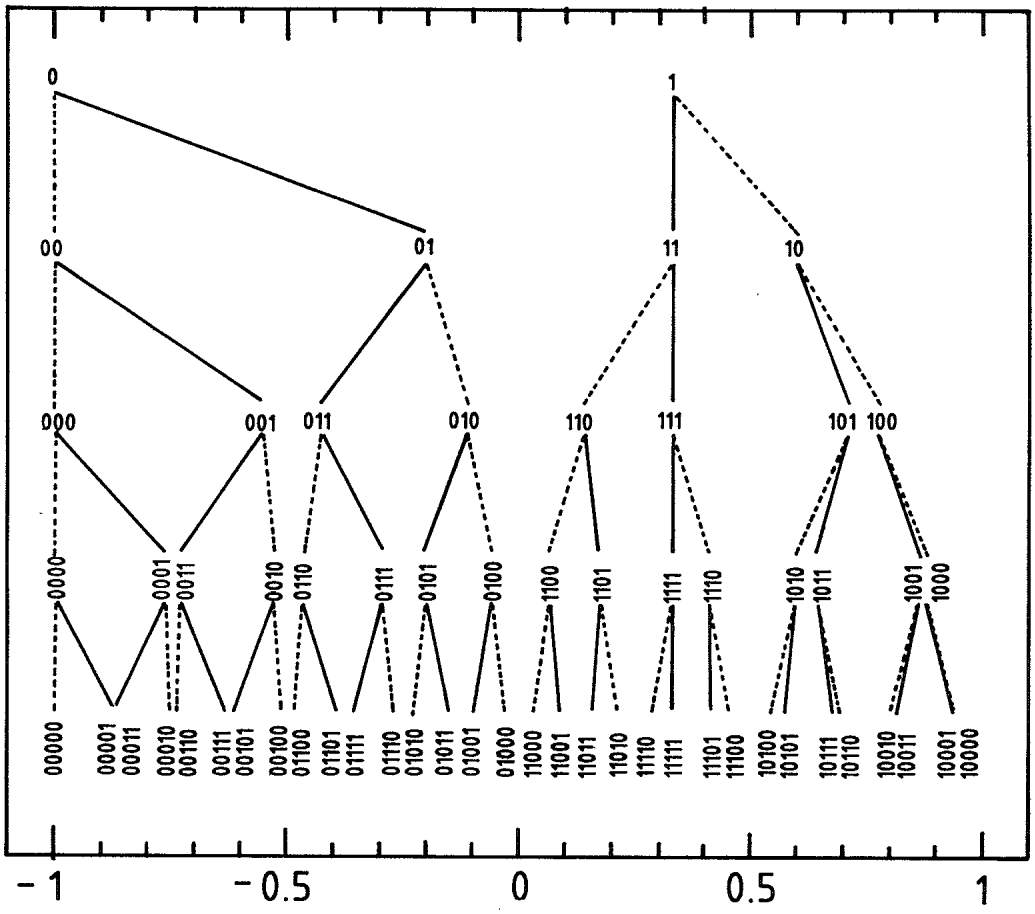

FIG. 2. Alternating binary tree that gives the order of itineraries in one-hump maps. The order is increasing from left to right. Thus $1>0$, but $11<10$, etc.

the points to the left of C mapped to the lower fold, and those to the right mapped on to the upper fold. Hence the immediate symbolic history of a point determines its transversal position on the coarsest scale.

The next iteration of f will stretch $f(D)$ by a factor of 2 and fold it back on itself. The folding relevant for the Hénon attractor (with $b>0$) is the following. The point 0 of Fig. 3(c) corresponds to the left fixed point of the Hénon map, whose smaller eigenvalue is negative. Hence $f(A)$ and A should be on opposite sides of 0. The folding that provides this is given in Fig. 3(d). It is easily checked that the symbolic history of points on a given fold is as shown in Fig. 3(d). As Fig. 1 shows, the same arguments are valid for the Hénon attractor (but with a slightly different partition of the plane, as will be described later).

The effect of the next iteration is shown in Fig. 3(e), and at this level of refinement the last three entries of the symbolic past are needed to determine the folding on which a point lies. The ordering of the folding can be determined by defining a coordinate δ analogous to γ of Sec. II A. First define d_k by

$$d_k=\sum_{i=1}^{k}(1-a_{-i})\ (\mathrm{mod}2)\ , \tag{2.6}$$

where $a_{-1},a_{-2},\ldots$ determines the symbolic past of a point. Then it is easily seen that $(1-0.d_1)$ is the vertical

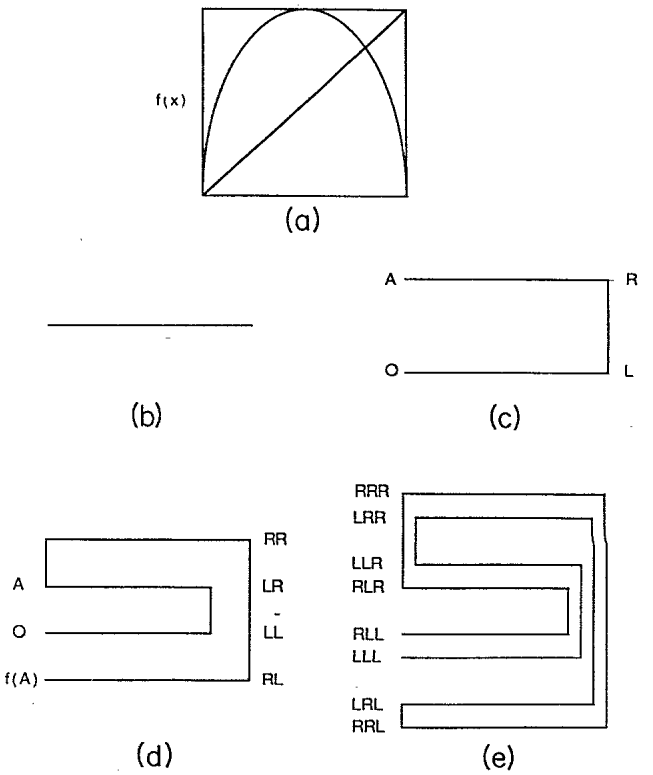

FIG. 3. Process of folding and the ordering of the folds by symbolic dynamics. See text for details.

position of the folds of Fig. 3(c), where the fraction is expanded in base 2. Similarly $(1-0.d_1d_2)$ is the vertical position of folds in Fig. 3(d), and $(1-0.d_1d_2d_3)$ that of folds in Fig. 3(e). In general, one defines

$$\delta=1-0.d_1d_2\ldots=1-\sum_{k=1}^{\infty} d_k 2^{-k}, \tag{2.7}$$

and then $\delta(x)$ will have the same cross sectional ordering as x.

Any point x on the attractor is thus represented by a pair of numbers $\gamma(x)$ and $\delta(x)$ defined, respectively, by the symbolic future and past of x. If b is negative, the attractor folds the stretched domain in a orientation-preserving way. The definition of δ is different (but again straightforward). Figure 4 shows how the γ-δ plane is constructed iteratively. This plane will be termed the symbol plane.

The symbolic sequence of a periodic point of period N has the form $(a_1,a_2,\ldots,a_N)^\infty$. Thus all the symbolic information (i.e., its symbolic history and future) can be encoded in a finite string. This renders the periodic points especially important for the description of the attractor. In particular, note that in Eqs. (2.4) and (2.6), $a_{N+k}=a_k$ and $a_{-k}=a_{N-k}$. Furthermore, the neighborhood of a periodic point is described by the linearization of the N times iterated map. Hence, as opposed to describing the strange attractor as a whole, we break it into neighborhoods of periodic points whose local structure is described by eigenvalues and eigenvectors of the periodic points. This is different from previous approaches[21] for estimating the size of the Hénon attractor, based on only two fixed points, and their unstable manifolds. The description in terms of periodic points is more democratic; instead of globally continuing the unstable manifolds, we piece the attractor together from small linear sections.

Iterating a point x by the map is (as will be shown in Sec. II C) equivalent to the application of an area preserving transformation on the γ-δ plane.

In the examples considered in the remainder of the paper each allowed periodic point will be marked by a dot in the symbol plane. The resulting picture will henceforth be called the symbol plane.

C. *D* transformation

The transformation $D:[0,1)\times[0,1)\to[0,1)\times[0,1)$

$$D(x,y)=\begin{cases}(2x,\frac{1}{2}[1-y)] & \text{if } x<\frac{1}{2}\\ (2-2x,\frac{1}{2}[1+y)] & \text{if } x\geq\frac{1}{2}\end{cases} \tag{2.8}$$

is the simplest map whose dynamics is similar to that de-

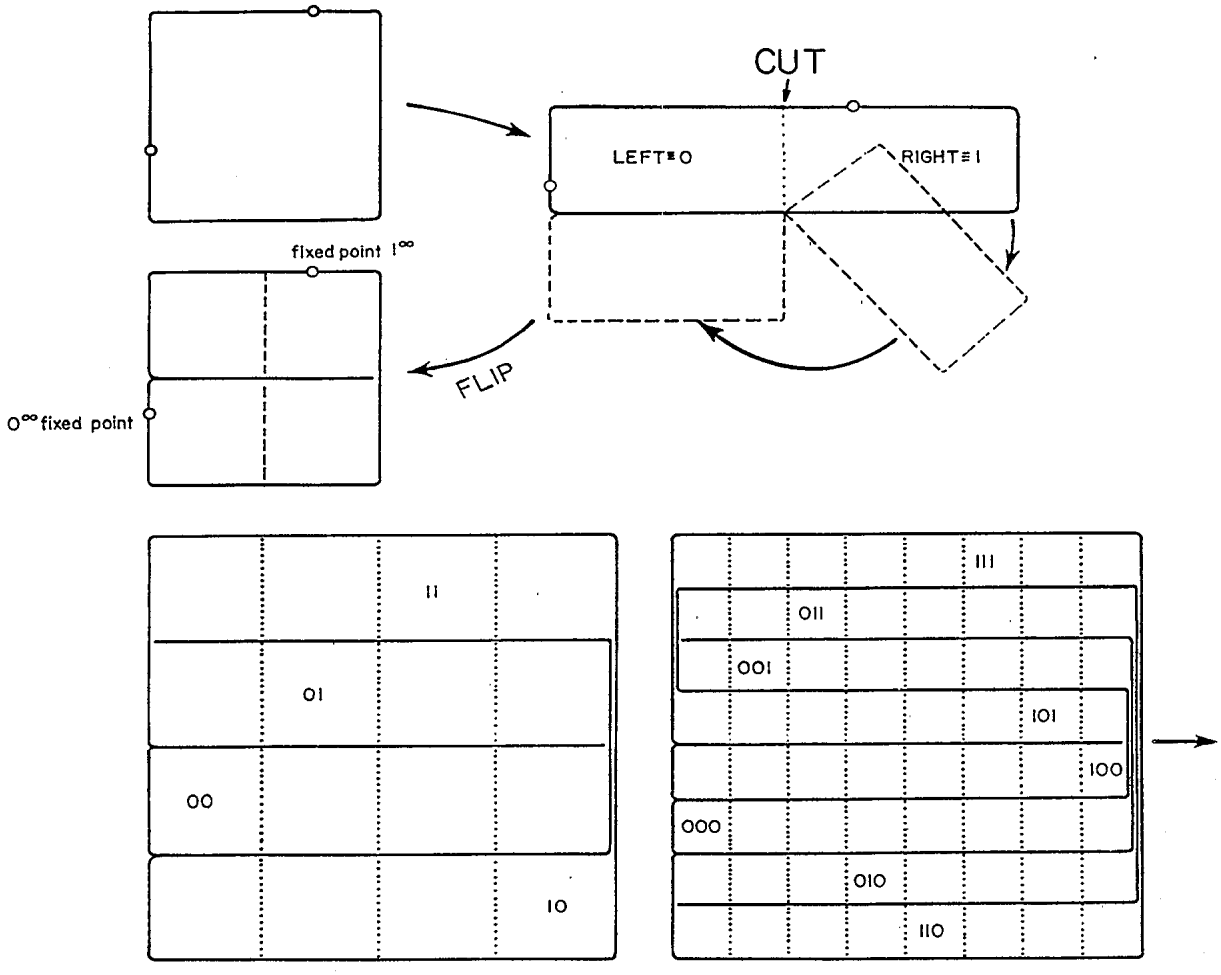

FIG. 4. Iterative construction of the symbol plane.

scribed in Sec. II B. We will first prove that the application of a Hénon-type map is equivalent to the action of D on the symbol plane. We will refer to this as the D transformation. Consider a point x whose symbolic past and future are

$$(\ldots,a_{-n},\ldots,a_{-2},a_{-1}) \text{ and } (a_1,a_2,\ldots,a_n\ldots) . \tag{2.9a}$$

The symbolic past and future of $f(x)$ is

$$(\ldots,a_{-n},\ldots,a_{-2},a_{-1},a_1) \text{ and } (a_2,a_3,\ldots,a_n\ldots) . \tag{2.9b}$$

Its abscissa on the symbol plane is

$$\bar{\gamma}=\sum_{k=1}^{\infty}\bar{c}_k 2^{-k} , \tag{2.10}$$

where

$$\bar{c}_k=\sum_{i=1}^{k}a_{i+1}(\text{mod}2)=\begin{cases}c_{k+1} & \text{if } a_1=0\\ 1-c_{k+1} & \text{if } a_1=1\end{cases} . \tag{2.11}$$

Hence

$$\bar{\gamma}=\sum_{k=1}^{\infty}\bar{c}_k 2^{-k}=\begin{cases}2\gamma & \text{if } a_1=0\\ 2-2\gamma & \text{if } a_1=1\end{cases} , \tag{2.12}$$

which is the first component of (2.8). It can similarly be shown that $\delta(x)$ maps as the second component of (2.8).

It follows that the coordinates of the periodic point of D with a given symbolic sequence is (γ,δ), where γ and δ are determined by (2.3) and (2.7). Thus D is the two-dimensional analog of the tent map (2.5).

As an application, consider a unimodal map which is Kupka-Smale complete[22] (i.e., a map that is onto the interval). For such a map all possible symbol sequences correspond to allowed periodic points, and hence the allowed points fill all of the symbol plane. If the map is not onto the interval (i.e., not Kupka-Smale complete), periodic points cannot have coordinates greater than the maximum of the map. Hence for all allowed periodic points

$$\gamma\le\gamma_0 , \tag{2.13}$$

where γ_0 is the coordinate evaluated from (2.3) and (2.4) using the itinerary of the extremum $\{a_k^{(0)}\}$. Thus the strip S_0 of the symbol plane for which $\gamma>\gamma_0$ will be empty. The set of disallowed regions S is the union of S_0 and all its images and preimages under D; see Fig. 5.

The strip S_0 consists of those symbol sequences whose itinerary begins with a subsequence whose γ coordinate is greater than γ_0, i.e., certain subsequences are prohibited at the head of the itinerary for allowed periodic points. Since S is the union of all these points and their shifts, this means that the allowed periodic points cannot contain certain subsequences in their itinerary. Alternately, the disallowed orbits are determined by the inclusion of symbol subsequences $\{\bar{a}_k\}$ in their itineraries such that $\gamma(\bar{a})>\gamma_0$.

Note finally that if the γ and δ coordinates are evaluated for a point on the attractor, then (γ,δ) should lie inside the allowed regions of Fig. 5.

D. The pruning front

The conclusion of Sec. II C is that in the one-dimensional case a strip (and all its iterates) were removed from the symbol plane. This simplicity arises from the fact that a single parameter sufficed to determine the symbolic dynamics completely. In the two-dimensional problem this line is replaced by what we refer to as the "pruning front."

A pruning front arises from the fact that the two-dimensional attractor is not a single curve, but is multisheeted. There is no single "maximal point" as in the one-dimensional case; each sheet defines a locally highest allowed itinerary. The pruning front is computed therefore by determining the "primary" sequence of homoclinic tangencies. The homoclinic tangencies are points where the unstable manifold and the stable manifold are tangent. "Primary" tangencies are those tangencies which lie closest to the y axis in Fig. 1. The primary sequence is that sequence which will be used to define the "good" partition[23] in Sec. II D 2, and has arisen from the two onto one folding of the plane to itself. The relation between the physical plane (Fig. 1) and the symbol plane (Fig. 4) is obtained by cutting the physical unstable manifold at homoclinic tangencies and straightening out the folds on the attractor. As parameters vary, the periodic orbits are shed off the attractor by inverse bifurcations, i.e., their unstable and stable manifolds lose their transverse intersection as they hit a homoclinic tangency. The picture that emerges therefore is that *every* primary homoclinic tangency cuts out a rectangle of forbidden itineraries in the symbol plane. Due to the foliation of the stable manifold, the rectangles so deleted build up a front which is monotone across half the symbol plane. What this means is that, in contradistinction to one-dimensional maps, in two-dimensional maps the symbolic dynamics is specified by infinity of parameters, one for each homoclinic tangency. The pruning front is not a line but a function with a discontinuity at every binary rational number.

We conjecture that the pruning front specifies the allowed symbolic dynamics (the union of all periodic points) fully; there are no orbits which are pruned out by other mechanisms. All the other disallowed regions of the symbol plane are obtained by backward and forward iterations of the primary pruned patch by the D transformation.

However, for a finite dissipation ($b<1$) the discontinuities in the pruning front shrink exponentially like b^n, where n is the length of the corresponding periodic orbits. On the coarsest scale the attractor consists of two sheets, whose separation is of $O(b)$, and on finer scales the separations are of $O(b^n)$; see Fig. 1. Hence, even though in principle there is infinity of parameters, to any finite accuracy the symbolic dynamics is well described by a finite number of rules. We shall illustrate this in Sec. II E.

To illustrate the above discussion we examine the symbolic planes of two maps, the Hénon map, and the Lozi

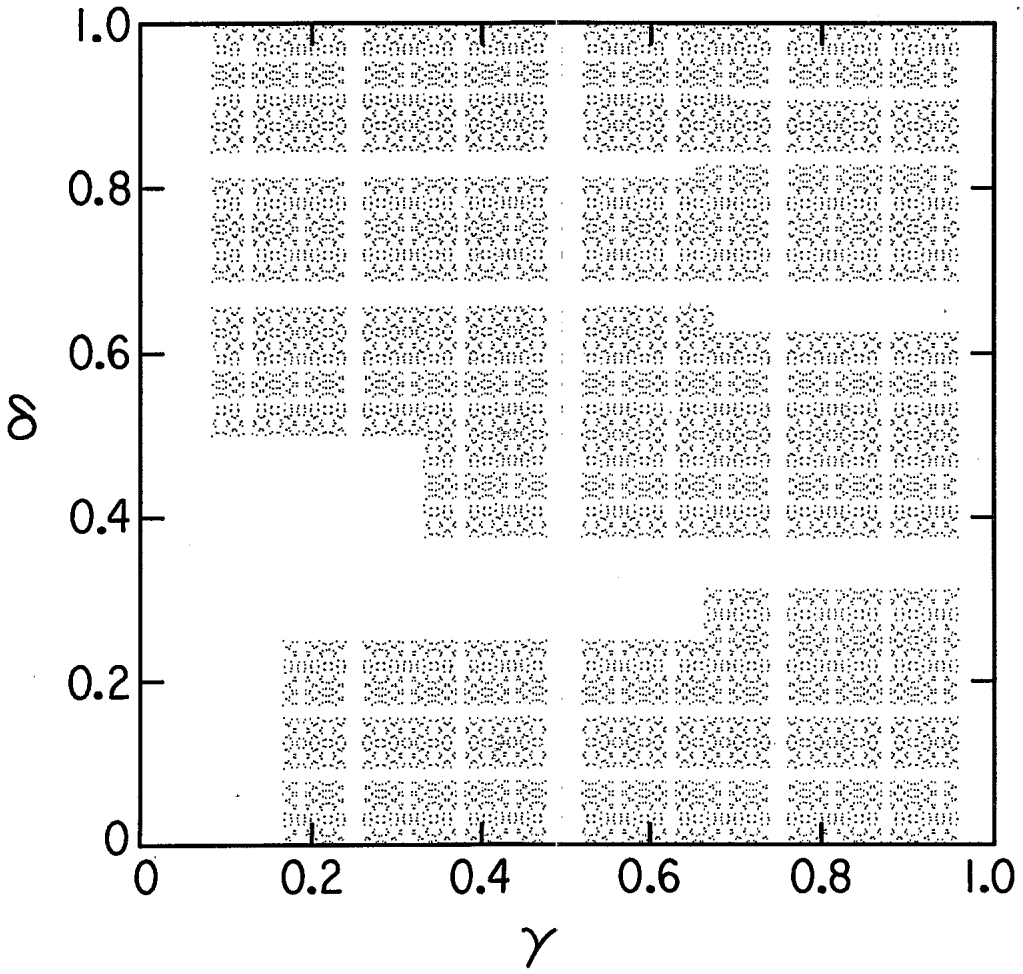

FIG. 5. Symbol plane for the map $x'=a-x^2$ for $a=1.9$. 15 178 points belonging to periodic orbits of length 15 are plotted.

map given by

$$x'=y+(a-1)-a\,|x|\ ,$$
$$y'=bx\ . \tag{2.14}$$

We begin by considering the Lozi map, since its piecewise linearity allows analytic calculations.

1. *Lozi map*

The iterates of (2.14) form a strange attractor for $a=1.7$ and $b=0.5$ (Ref. 24). We will first show that a partition of the plane by the y axis determines the periodic points uniquely through the symbolic sequences. We will then determine the form of the symbol plane for the attractor.

The partition of the plane by the y axis uniquely determines the periodic points; since (2.14) is linear for $x\geq 0$ and for $x<0$, given the symbolic sequence, one obtains a linear equation that needs to be solved for the periodic point, which hence leads to a unique solution. Thus the symbolic dynamics will contain an L for $x<0$, R for $x>0$, and a C for $x=0$.

The two-dimensional analog of the Kupka-Smale complete map is a map at the crisis point.[25] It is the largest value of $a(b)$ for which a strange attractor exists. At the crisis point there is a heteroclinic tangency of the unstable manifold of the 1^∞ fixed point with the stable manifold of the 0^∞ fixed point. For the Lozi map it is given by $a=(2-\frac{1}{2}b)$.[26]

As b increases along the crisis line, some orbits disappear through inverse tangent bifurcation. For the Lozi attractor this is equivalent to a point in the orbit crossing the y axis. As b increases from 0, the points that cross the axis are those which were close (say within a distance ϵ) to it at $b=0$. But all such points need not cross the axis since some of them may move away from the axis with increasing b. It is shown in Appendix B that to linear order in b the points that do cross the axis are those whose preimages lie to the left of the critical point and were closer than a distance $\epsilon(b)\sim b$ from the axis. Hence on the symbol plane the bottom half strip S_0 about $\gamma=\frac{1}{2}$ whose width is $\epsilon(b)$ will not contain periodic points. Once again periodic points are disallowed inside the images and preimages of S_0. In Fig. 6(b) we show the symbol plane computed for $a=1.75$ and $b=0.5$ (which is a crisis point), and it indeed agrees with the theoretical result. Note that the image $D(S_0)$ of S_0 is a half strip on the right end, the periodic points inside of which will have a tail LX where X is either L or R. Hence once again the disallowed orbits are determined by the pres-

ence of certain subsequences. In this case the head $\{\bar{a}_k\}$ of points in $D(S_0)$ should have $\gamma(a)>\gamma_0$ and their tail should have the form LX. Thus the symbolic subsequence $LX\{\bar{a}_k\}$ is prohibited in any allowed periodic orbit.

For an attractor below crisis, additional periodic points are missing, corresponding to those that were missing for the incomplete unimodal map. The empty regions in the symbol plane in this case will be approximately the superposition of empty regions of the last two examples; see Fig. 7. Notice that even for b values as high as $b=0.5$, the largest discontinuity in the pruning front is clearly visible, but the smaller ones are difficult to see. This fact will be used to produce an efficient finite grammar for the union of all periodic points in Sec. II E.

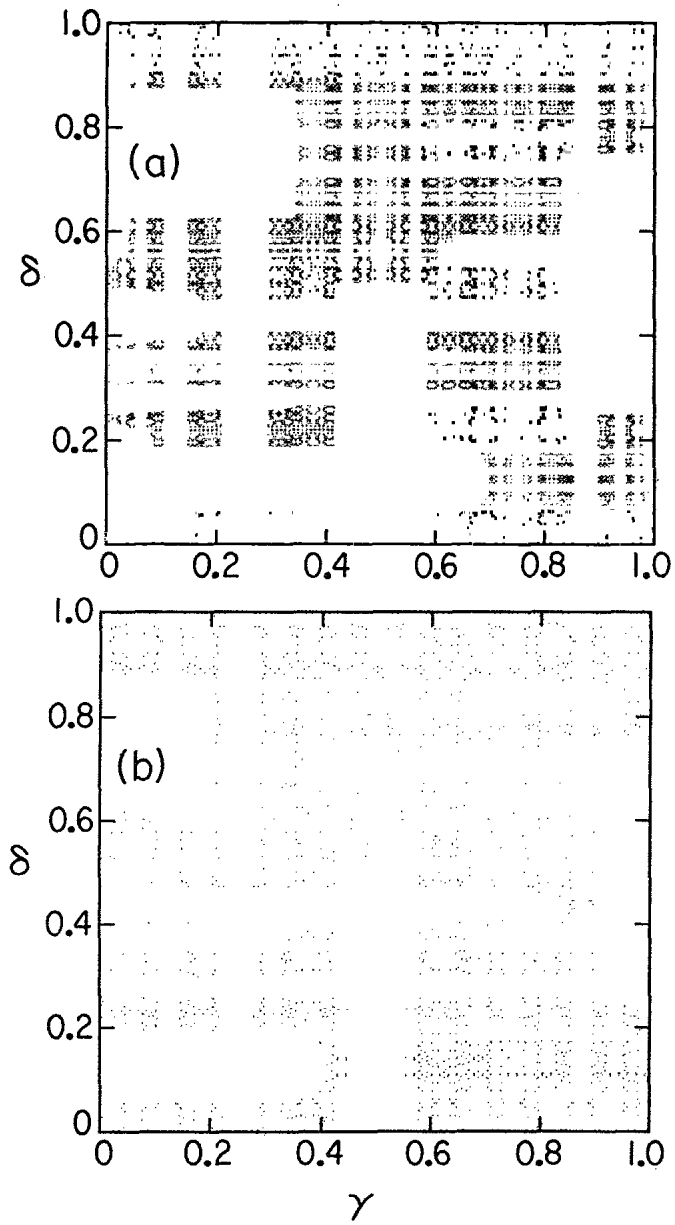

FIG. 6. Symbol planes of Hénon and Lozi maps at crisis. (a) Hénon map with $a=1.803\,241\ldots, b=0.1$. (b) Lozi map with $a=1.9, b=0.2$.

2. *Hénon attractor*

The results of Sec. II D 1 carry over to the Hénon attractor. We first explain that for periodic points to be determined uniquely by the symbolic sequences, the plane has to be partitioned by the homoclinic tangencies. We then show numerically that the symbol plane for the Hénon attractor has the same form as that for the Lozi attractor, and finally use the results to organize the orbits on well-ordered trees.

A partition of the plane by the y axis does not determine the periodic points uniquely. Numerically it appears that a line joining the homoclinic tangencies does in fact partition the plane as needed.[23] It is easy to see that an unstable periodic point cannot cross this line. If one did, then at the point of crossing its eigenvalues have to be equal and hence (since their product b^N is smaller than 1) each has to be inside the unit disk; i.e., the orbit is stable. Hence as long as the orbits are unstable, they cannot cross the line of homoclinic tangencies, and we conjecture that this line partitions space so that the unstable periodic points are uniquely described by symbolic sequences. Numerically the partition appears to determine the periodic points uniquely for periods up to 20. The partition again defines an L for x to the left of the partition, R for an x to the right, and C if x falls on the partition.

The symbol plane for the crisis point at $b=0.1$ ($a=1.803\,241\ldots$) is shown in Fig. 6(a) which is qualitatively identical to Fig. 6(b). For the parameters considered by Hénon ($a=1.4, b=0.3$) the symbol plane is shown in Fig. 8, which is similar to Fig. 7. We conclude that the allowed and disallowed periodic orbits are well described by the pruning front in the symbol plane.

E. Growing periodic orbits on well-pruned binary trees

1. *The Grammar*

For any $b>0$ and smaller than its crisis value, the number of periodic points of period n is smaller than 2^n. Thus although the orbits can be always put on a binary tree, this tree is incomplete, and rules for its pruning should be found. In this section we show how to find such rules for well chosen points in parameter space. The main result is that for such points, and b small enough, such trees are universal, predicting correctly the number of periodic points for length n which is not too large in all Hénon-like mappings.

The fundamental ingredients that allow a construction of a tree from local rules are the following.

(i) For $b=0$ the orbits are ordered along the a axis in a b-a plane according to the value of the number γ calculated from their itinerary according to Eq. (2.7). This means that as a is decreased from its crisis value [$a=2$ for (1.1) and $b=0$], the orbits that are shed off the attractor are all those whose $\gamma>\bar{\gamma}(a)$, where $\bar{\gamma}(a)$ is the maximal value.

(ii) For $b>0$ some orbits disappear at values of a, $a(b)$, which are smaller than their $a(0)$, and others at larger values. The rules were derived in Sec. II D 1, and are correct for small b: orbits whose itineraries finishes with

LX survive until $a=a(b)>a(0)$, whereas orbits whose itinerary finishes with RX disappear earlier, at $a=a(b)<a(0)$. For small b the b-a diagram looks as in Fig. (9), where the value of (b,a) for which the orbits are superstable is plotted. The essential property is that there are no intersections among the lines with the same slant, as long as b is small enough. Of course, lines with a right slant can intersect lines with a left slant. In the vicinity of these intersection points we can construct easily the local rules for the topology.

Consider, for example, an intersection point of the superstability line (more appropriately for $b\neq 0$ the line where the itinerary of the orbits contains a C) of a period 3 with itinerary RLC and a period 5 with itinerary $RLLRC$. The lines with the intersection point are depicted in Fig. 9, and we shall denote them by S_3 and S_5, respectively. We know that to the right of S_3, all the orbits that begin with RLL (i.e., just larger than RLC) and end with an LX ($X=L$ or $X=R$) are prohibited. Thus all the sequences

$$(RLL\ldots LX)^{\infty} \tag{2.15}$$

are prohibited. We can satisfy this requirement by disallowing the block of symbols $LXRLL$ from any itinerary. (We use the periodicity.)

In addition to the left of S_5 we cannot find any orbit whose itinerary begins with a head larger than $RLLRC$. Hence (using periodicity) no itinerary containing any of the blocks

$$RLLLL, RLLLR, RLLRR \tag{2.16}$$

is allowed.

The condition that disallows $LXRLL$ removes the region A from the symbol plane (see Fig. 10). The conditions (2.16) remove the strip B, as shown in Fig. 10. At the intersection point the symbol plane should be given by Fig. 10 in addition to all the images and preimages of the disallowed regions. The symbol planes for three different Hénon-type maps (see Sec. II E 3 below) with parameters corresponding to this very same intersection point are shown in Fig. 11.

2. *Construction of the tree*

At its nth level, the well-pruned tree should have all the paths that do not contain the disallowed sequences. Irrespective of the question of which are the disallowed blocks of symbols (whether of the example of Sec. II E 1 or not) we can adopt the following strategy: let L and R have values 0 and 1, respectively. Assign a binary num-

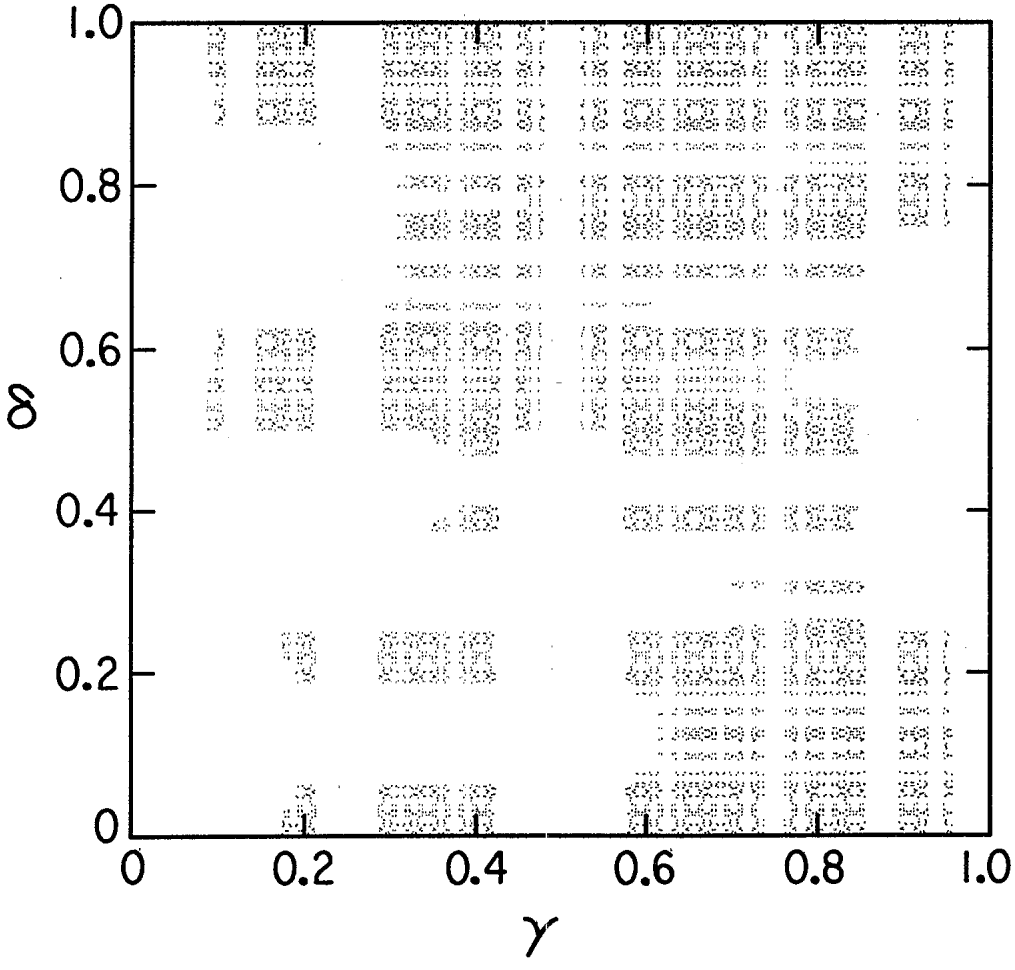

FIG. 7. Symbol plane for the Lozi map below crisis. $a=1.8, b=0.2$.

ber η to any itinerary of length n,

$$\eta=\sum_{i=1}^{n} a_i 2^{i-1} , \tag{2.17}$$

where

$$a_i=\begin{cases}1 & \text{if } R\\ 0 & \text{if } L\end{cases} . \tag{2.18}$$

All that we need to know is which of the 2^n binary numbers which are generated from all the possible itineraries are allowed. Consider again the example of Sec. II E 1. The disallowed sequences are 00100, 01100, 10000, 10001, and 10011. These have values of

$$4,\ 6,\ 1,\ 17,\ \text{and}\ 25 , \tag{2.19}$$

respectively. Form now from all the numbers $\eta=1$ to 2^N the numbers η_k, $(k=1,2\ldots,n-5)$,

$$\eta_k=\left[\frac{\eta \bmod 2^{k+5}}{2^k}\right]$$

$$=a_k+a_{k+1}2+\ldots+a_{k+4}2^n=b_1b_2b_3b_4b_5 . \tag{2.20}$$

If η_k equals any of the numbers (2.14), η is knocked out. This test is almost complete. It only fails to recognize sequences where the head and the tail combine to give such a number (such a path is disallowed by permutation). To overcome this difficulty we perform the test on the numbers $a_1,a_2,\ldots,a_na_1a_2a_3a_4$ rather than on $a_1\ldots,a_n$.

3. Results

We tested the predictions of the tree constructed in Sec. II E 2 against the three dynamical systems, i.e., Lozi, Hénon, and

$$X'=y+a\cos(\pi x/2)-1 ,$$
$$Y'=bx . \tag{2.21}$$

The parameters for the crossing point of the 3 and 5 cycles are $a=1.812\,579\,7, b=0.022\,864\,3$ for the Hénon map, $a=1.694\,697\,8$ and $b=0.064\,262\,3$ for the Lozi map, and $a=1.905\,870, b=0.030\,79$ for the map (2.21). We found the periodic orbits in these three maps by Newton-Raphson techniques and the numbers of periodic points in the tree and in these systems are presented in Table I. As we see, the number of periodic points pre-

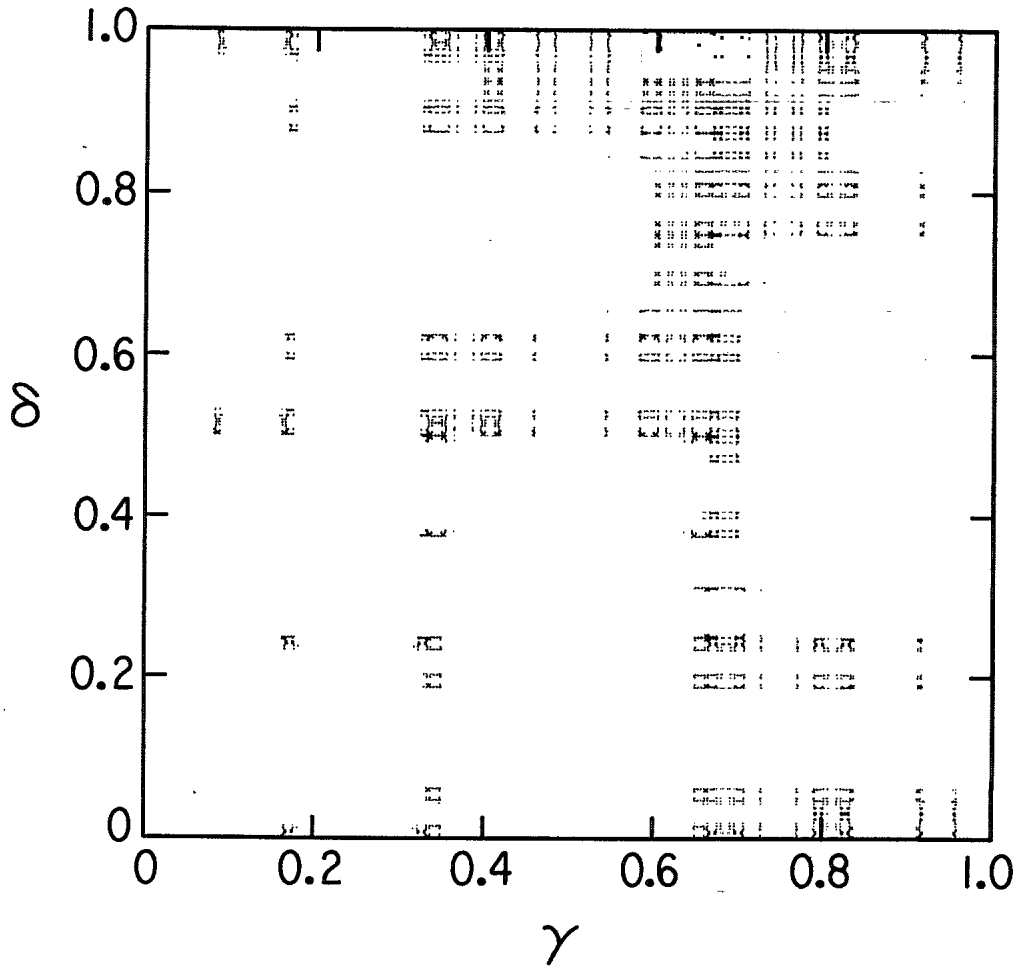

FIG. 8. Symbol plane for the Hénon map at the classical parameter value $a=1.4, b=0.3$. Notice that in this case a second discontinuity in the pruning front is clearly visible.

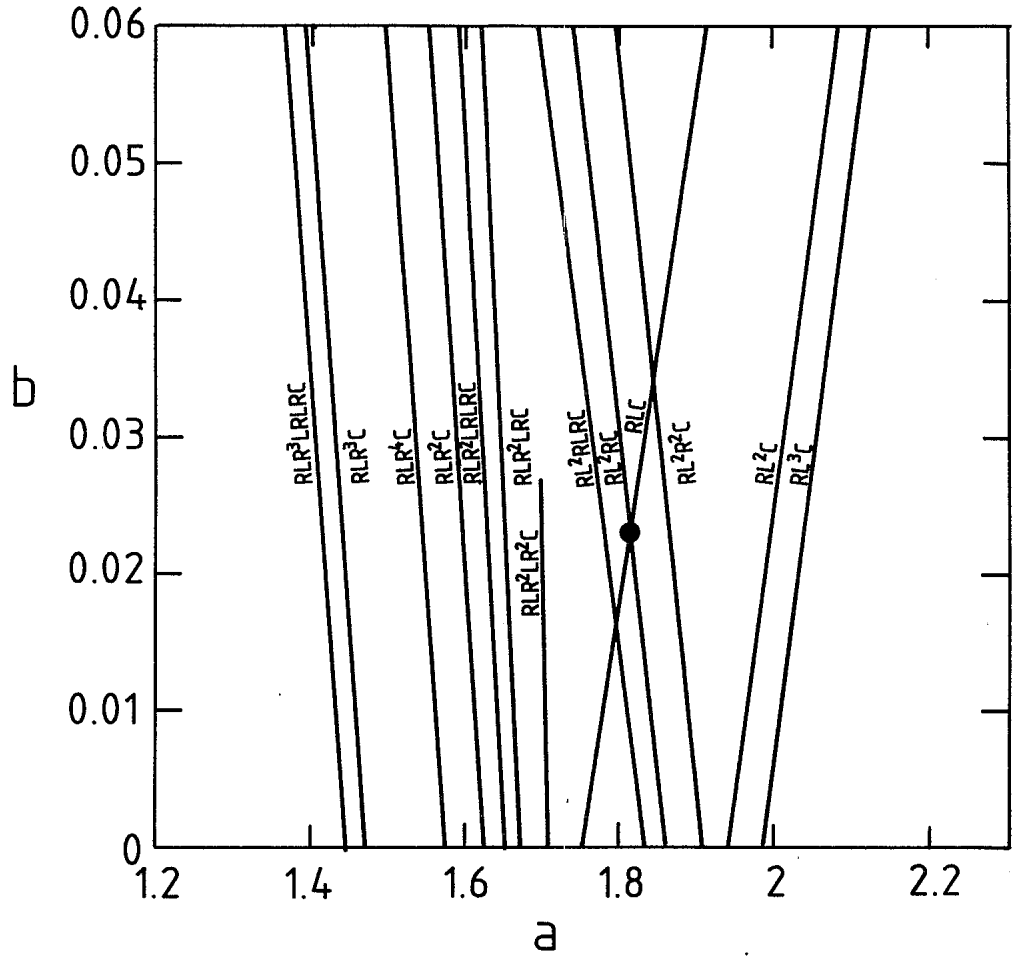

FIG. 9. The a-b parameter plane of Hénon map for small b. The lines are parameter values where the itineraries of the denoted orbits contain a C. Orbits whose itineraries end with $LC(RC)$ move to the right (left). We focus on the intersection of RLC and RL^2RC as an example.

dicted by the grammar agrees exactly with the number found in the Hénon map and in the Sin map (2.21). The Lozi map has more points sometimes. The reason is that in the Lozi map there is no cascade of period doubling, but period-doubled orbits begin simultaneously. Thus, for example, a period 3 exists together with its doubled 6,

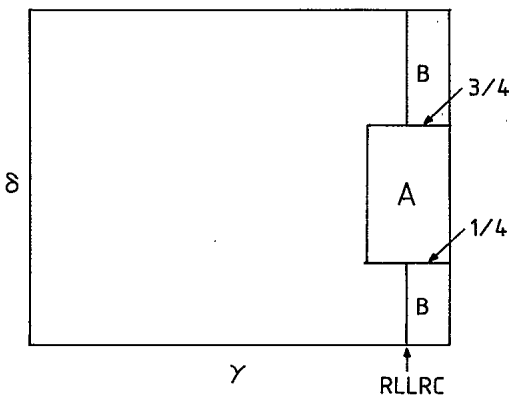

FIG. 10. Schematic pruning front for the point of intersection of Fig. 9. The region denoted by A is pruned by disallowing itineraries to contain block of the type $LXRLL$, whereas the strip B is pruned by disallowing blocks larger than $RLLRC$.

and thus there are 28 rather than 22 periodic points of length 6. Taking this into account yields exact agreement with the tree also in the Lozi case.

The availability of local rules for the pruning of the tree also means that we can calculate the topological entropy of the map. The topological entropy K_0 can be calculated for all practical purposes from the rate of increase of the number of allowed periodic points belonging to orbits of length n. Denoting this number by N_n, we write

$$N_n \sim e^{K_0 n}, \quad n \to \infty \ . \tag{2.22}$$

An nth-order approximant to K_0 can be calculated from the well-pruned tree as

$$K_0^{(n)} = \frac{\ln N_n}{n} \ . \tag{2.23}$$

These approximants are displayed in Table I. It is interesting to compare this approximant to a calculation based directly on the available rules. The most straightforward calculation is completed via the transfer matrix formalism.[27] In this formalism we consider a matrix

$$T_{a_1 \ldots, a_{n-1}, a_2', \ldots, a_{n-1}' a_n} \ ,$$

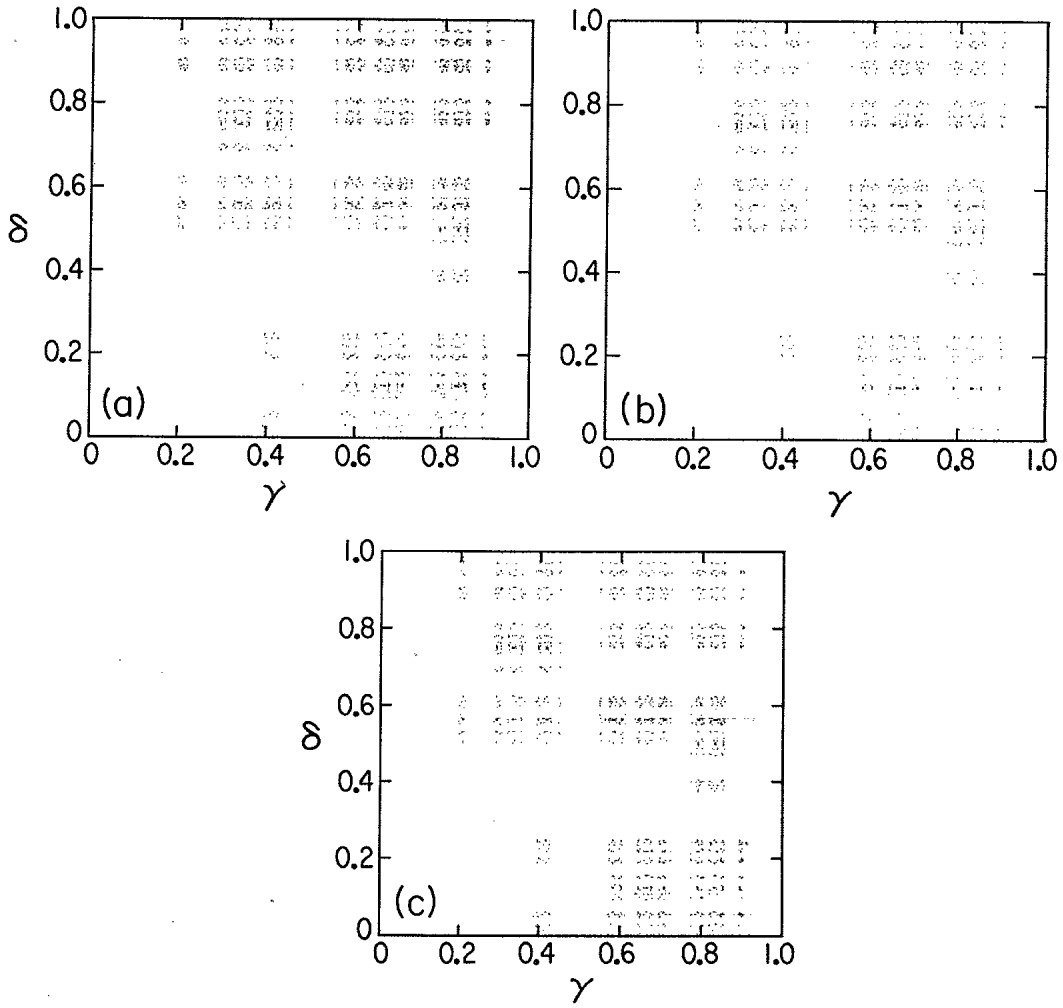

FIG. 11. Symbol planes of the Hénon (a), Lozi (b), and the map (2.21) (c), at their parameter values of the intersection point of Fig. 10. The parameters are given in the text. Notice the (b) contains more points, for reasons explained in the text. The symbol planes (a) and (c) are identical, and to this order of cycles ($n \leq 15$) are universal.

TABLE I. The number of periodic points belonging to periodic orbits of length n in Hénon-type maps. The second column is the theoretical value expected from the universal grammar. See text for explanation of the differences with the Lozi map. The last column is the nth-order approximant of the topological entropy.

Period	Tree	Hénon	Sin	Lozi	$K_0^{(n)}$
6	22	22	22	28	0.515 17
7	44	44	44	44	0.540 60
8	64	64	64	64	0.519 86
9	116	116	116	134	0.528 18
10	194	194	194	204	0.526 79
11	310	310	310	310	0.521 51
12	542	542	542	584	0.528 61
13	886	886	886	886	0.522 06
14	1516	1516	1516	1516	0.523 13
15	2548	2548	2548	2698	0.522 87

which is defined according to

$$T_{a_1,\ldots,a_{n-1},a'_2,\ldots,a'_{n-1},a_n} = \gamma(a_1,\ldots,a_n)\delta a_2 a'_2,\ldots,\delta a_{n-1},a'_{n-1}\,, \tag{2.24}$$

where

$$\gamma(a_1,\ldots,a_n)=\begin{cases}1 & \text{if } a_1\ldots,a_n \text{ is an allowed block}\\ 0 & \text{if } a_1,\ldots,a_n \text{ is an excluded block}\,.\end{cases} \tag{2.25}$$

In the case considered above, the blocks $a_1,\ldots,a_n$ are of length 5, meaning that T is a 16×16 (sparse) matrix. In the notation of Eq. (2.18), this matrix in the present case is

$$T=\begin{bmatrix} 1^2 & 0^{14} & \\ 0^2 & 1^2 & 0^{12} \\ 0^5 & 1 & 0^{10} \\ 0^6 & 1^2 & 0^8 \\ 0^8 & 1^2 & 0^6 \\ 0^{10} & 1^2 & 0^4 \\ 0^{13} & 1 & 0^2 \\ 0^{14} & 1^2 & \\ 0^{16} & & \\ 0^2 & 10^{13} & \\ 0^4 & 1^2 & 0^{10} \\ 0^6 & 1^2 & 0^8 \\ 0^8 & 1^2 & 0^6 \\ 0^{10} & 1^2 & 0^4 \\ 0^{12} & 1^2 & 0^2 \\ 0^{14} & 1^2 & \end{bmatrix}, \tag{2.26}$$

where we have used a shorthand notation for the rows, in which the second row for example is 0011000000000000. The topological entropy should be (asymptotically) the logarithm of the largest eigenvalue of this matrix. Computing this eigenvalue, we find

$$K_0=0.522\,737\,64\ldots . \tag{2.27}$$

Evidently, the approximants tabulated in Table I appear to converge to this value.

III. METRIC PROPERTIES AND SCALING EXPONENTS

The organization of the strange attractors about their unstable periodic orbits can be used also to calculate their metric properties in a systematic and efficient way. We base the analysis on the spectrum of singularities $[f(\alpha)]$ formalism.[6] In this formalism one uses the natural ergodic measure generated by the time series $\{\mathbf{X}_i\}_{i=1}^N, \mathbf{X}_i=(X_i, Y_i)$. Then the measure $P_n(l_1,l_2)$ in a box of size $l_1\times l_2$ centered around $\mathbf{X}_n$ is considered, where l_1 and l_2 are in the direction of the local eigenvectors calculated from the tangent map around $\mathbf{X}_n$. This measure is defined by[9,10,28]

$$P_n(l_1,l_2)=\lim_{N\to\infty}(1/N)\sum_{i=1}^{N}E_n(\mathbf{X}_i) , \tag{3.1}$$

where

$$E_n(\mathbf{X})=\begin{cases} 0 & |\xi|>l_1 \text{ or } |\eta|>l_2 \\ 1 & |\xi|<l_1 \text{ and } |\eta|<l_2 \end{cases} \tag{3.2}$$

and

$$X-X_n=\xi\bar{e}_1(n)+\eta\bar{e}_2(n) , \tag{3.3}$$

where $\bar{e}_1$ and $\bar{e}_2$ are the eigenvectors of J_n. The fundamental scaling hypothesis is that $P_n(l_1,l_2)$ scales like[9,10,15]

$$P_n(l_1,l_2)\sim l_1^{\alpha_1}l_2^{\alpha_2} . \tag{3.4}$$

The relation to the more usual[6] isotropic scaling $P(l)\sim l^\alpha$ is obtained for $l_1=l_2$, leading to $\alpha=\alpha_1+\alpha_2$. The nonisotropic scaling (3.4) is required in the case of strange attractors, where the scaling exponents in the unstable direction are very different from those in the stable direction.

Next one wants to know the range of α, $\alpha_{\min}<\alpha<\alpha_{\max}$, and how many times $N(\alpha)\Delta\alpha$ one finds α between α and $\alpha+\Delta\alpha$. Naturally, this number depends on the length scale l. To scale this trivial dependence out one uses $f(\alpha)$ defined by

$$N(\alpha)\Delta\alpha\sim l^{-f(\alpha)}\Delta\alpha . \tag{3.5}$$

The $f(\alpha)$ function is taken as a convenient summary of the scaling properties of the set. Clearly, a scheme to connect the nonisotropic scaling (3.4) (which is essential) to the single length-scale dependence (3.5) is needed. Such a scheme is offered by the partition function formalism.[6] We shall cover the attractor with balls of radius l_i (nonconstant l_i varies from place to place) and calculate the measure P_i of each box. Then we shall consider the partition function

$$\Gamma(q,\tau)=\sum_i\frac{P_i^q}{l_i^\tau} . \tag{3.6}$$

It has been shown that in the limit of increasingly fine partitions the condition $\Gamma(q,\tau)=1$ singles out a quantity $\tau(q)$ such that

$$\alpha=\frac{\partial\tau(q)}{\partial q},\quad f(\alpha)=q\frac{\partial\tau(q)}{\partial q}-\tau(q) . \tag{3.7}$$

The nonisotropy of the set enters into such a calculation through the coverage of the natural oblong partitions by balls whose radii are the narrow sides of the oblong shapes.

Of particular interest will be apparent nonanalyticities which can appear in $f(\alpha)$ in Hénon-type mappings. We shall suggest that these nonanalyticities, which can be interpreted as phase transitions in the thermodynamic formalism of multifractals,[29,30] are absent in hyperbolic attractors like the Lozi attractor. They appear due to the existence of homoclinic tangencies (the Newhouse phenomenon).[31]

The analysis of the metric properties will be performed using tools, some of which have only recently been developed. Therefore we review the needed background material first.

A. Periodic orbits and scaling exponents

The basic assumption is that the metric properties of the invariant measure can be calculated once the properties of the periodic orbits are known. The important property of the periodic orbits is their stability. Denoting the tangent map about a point $\mathbf{X}_i$ on the attractor by J_i, we calculate the stability of an orbit of length $n, \mathbf{X}_1, \mathbf{X}_2 \ldots, \mathbf{X}_n$ from the eigenvalues μ_1,μ_2 of the matrix J,

$$J=J_n\ldots J_2J_1 . \tag{3.8}$$

The Lyapunov exponents are defined as

$$\lambda_{1,2}^{(n)}=\ln\mu_{1,2} . \tag{3.9}$$

The convention will be that $|\lambda_1|>1$ and $|\lambda_2|<1$.

The relation between the periodic orbits and the invariant measure is obtained when one realizes that the probability to see a particular orbit of length n is proportional to $\exp(-\lambda_i^{(n)})$. We assume that better and better approximants to the invariant measure $\rho(\mathbf{x})$ are obtained by looking at all the periodic points belonging to periods of increasing length n. Denoting the set of periodic points of length n by Fix(n) we write[10,32]

$$\rho(\mathbf{x})=\sum_{\mathbf{y}\in \mathrm{Fix}(n)} \delta(\mathbf{x}-\mathbf{y}) e^{-\lambda_1^{(n)}(\mathbf{y})} \Big/ \sum_{\mathbf{y}\in \mathrm{Fix}(n)} e^{-\lambda_1^{(n)}(\mathbf{y})} . \tag{3.10}$$

The eigenvalues of the periodic orbits yield the scales l_i and measures P_i of (3.6). As discussed in Sec. II, the forward iterate of a Hénon-type map generates folds of the attractor. After nth iteration each fold contains (at most) one periodic point of cycle length n. The thickness of the fold is determined[8] by the contracting eigenvalue $\exp[\lambda_2(n)]$. The length of the fold is of $O(1)$.

If we assume that the attractor is hyperbolic (i.e., approximates the folds by straight sections, and ignore the turnbacks), under iteration the expansion along the fold is approximated by the periodic point expanding eigenvalue $\exp(-\lambda_1^{(n)})$. We can cover the fold with $1/\exp(\lambda_2^{(n)})$ square boxes, each with measure $\exp[-\lambda_1(n)]\exp(\lambda_2^{(n)})$. So for hyperbolic attractors (3.6) becomes

$$\sum_{\mathrm{Fix}(n)} \frac{1}{e^{\lambda_2^{(n)}}} \frac{(e^{-\lambda_1^{(n)}} e^{\lambda_2^{(n)}})^q}{e^{\lambda_2^{(n)}\tau}} = \sum_{\mathrm{Fix}(n)} \frac{e^{-\lambda_1^{(n)}q}}{e^{\lambda_2^{(n)}(\tau-q-1)}} = 1 . \tag{3.11}$$

However, this is too crude for nonhyperbolic attractors. Every fold of an attractor ends in a turnback, and on turnbacks stability is marginal, and the measure is singular. Hence we need to refine the unstable direction as well. Realizing that the periodic points are also owned by the map run backwards, we use the local scales $1/e^{\lambda_1^{(n)}}$, which are the contraction rates of the inversely run orbits, to define strips "orthogonal" to the previous ones.[10]

The horizontal strips are now given an address which is the itinerary of the periodic point, whereas the vertical strips are associated with the itineraries run backwards. Every box in this partition is identified by an itinerary of $2n$ symbols R,L; see Fig. 12.

What remains now is to estimate the measure of each box. Evidently, not every box contains at this stage periodic points; in fact, most of them are empty. To overcome this we look now at all the periodic points of length $2n$. Each of these is equipped with an itinerary of $2n$ symbols, which we consider as head and tail of n symbols, respectively. By matching the head and tail of the address to vertical and horizontal strips, respectively, we assign a periodic point of length $2n$ to any box that matches the itinerary of the $2n$ points. We know that

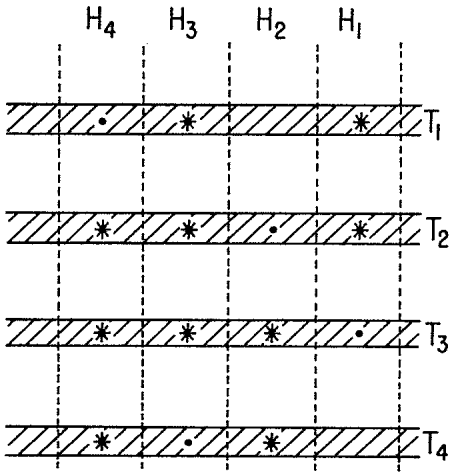

FIG. 12. The schematic covering of an attractor by boxes whose width and length are determined by the eigenvalues of the periodic points belonging to orbits of length n (denoted by dots). Every box has an address (H,T) which is obtained from the itineraries of these points. To estimate the measure, we find periodic points of length $2n$ whose itinerary is (H,T) (denoted by stars). The measure is then estimated from $\exp[\lambda_1^{(2n)}(H,T)]$.

there can be at most one point in each box, and some boxes are still left empty. The empty boxes are assigned zero measure, whereas the boxes that contain a periodic point are assigned a probability proportional to $\exp(-\lambda_1^{(2n)})$. P_i and l of Eq. (3.6) are obtained now by covering each box of Fig. 12 by $\exp[-\lambda_1^{(n)}(H)/e^{\lambda_2^{(n)}(T)}]$ square boxes of edge $l=\exp[\lambda_2^{(n)}(T)]$, each with a measure

$$\exp[-\lambda_1^{(2n)}(H,T)]\exp[\lambda_1^{(m)}(H)]\exp[\lambda_2^{(n)}(T)] .$$

In addition to this global description of the scaling properties, we can find direct relationships between the local scalings α_1,α_2 of Eq. (3.4) and the Lyapunov numbers of the orbits.

Remember the definition of the invariant measure (3.1). We make use now of the fact[9] that close to any point X_n of the attractor there exists a point belonging to some periodic orbit of length, say, m. Thus $X_{m+n}=X_n$, and from (3.1)

$$P_{n+m}(l_1,l_2)\approx P_n(l_1,l_2) . \tag{3.12}$$

On the other hand, after m iterations the original box $l_1\times l_2$ has been deformed to one of size

$$(l_1 e^{\lambda_1^{(m)}} \times l_2 e^{\lambda_2^{(m)}}) .$$

Using the preservation of probability,

$$\begin{aligned} P_{n+m}(l_1,l_2) &= P_n(l_1 e^{-\lambda_1^{(m)}}, l_2 e^{-\lambda_2^{(n)}}) \\ &= l_1^{\alpha_1} l_2^{\alpha_2} \exp(-\alpha_1\lambda_1^{(m)}-\alpha_2\lambda_2^{(m)}) , \end{aligned} \tag{3.13}$$

where in the last step Eq. (3.4) has been used. Collecting equations (3.4), (3.12), and (3.13) we conclude that[9]

$$\lambda_1^{(m)}\alpha_1+\lambda_2^{(m)}\alpha_2=0 . \tag{3.14}$$

To get a second equation in α_1 and α_2 we use Fig. 12 again. Since the edge sizes and the measure of each box is known, we can write Eq. (3.4) as

$$\exp[-\lambda_1^{(n)}(H)]^{\alpha_1}\exp[\lambda_2^{(n)}(T)]^{\alpha_2}\sim\exp[-\lambda_1^{(2n)}(H,T)] . \tag{3.15}$$

This equation can be written as

$$-\lambda_1^{(n)}(H)\alpha_1+\lambda_2^{(n)}(T)\alpha_2=-\lambda_1^{(2n)}(H,T) . \tag{3.16}$$

At this point we can rewrite Eq. (3.14) as

$$\lambda_1^{(2n)}(H,T)\alpha_1+\lambda_2^{(2n)}(H,T)\alpha_2=0 , \tag{3.17}$$

since the boxes are defined around $2n$ orbit points. The local description will give useful information that is difficult to see in the global theory.

B. Metric properties of the Lozi attractor

We considered the Lozi attractor at the parameter values $a=1.7, b=0.5$. Having located the periodic orbits, and having calculated their stabilities, we solved Eqs. (3.16) and (3.17), with n ranging from 6 to 10. Invariably, α_1 is found to be very close to 1. This is hardly surprising, since the Lozi attractor is hyperbolic. In terms of the eigenvalues, this means that roughly $\lambda_2^{(2n)}\sim 2\lambda_1^{(n)}$. Substituting this in Eq. (3.17) and subtracting from Eq. (3.16) results in

$$-2\lambda_1^{(n)}\alpha_1\approx-\lambda_1^{(2n)}\approx-2\lambda_1^{(n)} \tag{3.18}$$

or $\alpha_1=1$. Using this in Eq. (3.17), we find

$$\alpha_1^{(n)}=-\frac{\lambda_1^{(n)}}{\lambda_2^{(n)}} \tag{3.19}$$

and

$$\alpha^{(n)}=1-\frac{\lambda_1^{(n)}}{\lambda_2^{(n)}} . \tag{3.20}$$

Each periodic orbit contributes one α value to the spectrum with a multiplicity that is the order of the orbit.

The meaning of $\alpha_1=1$ is that the measure is uniform in the unstable direction. We can therefore use Eq. (3.11) to calculate $\tau(q)$. The singularity spectrum which is the Legendre transform of τ_q can now be evaluated. It converges as a function of n, and agrees very well with results obtained earlier.[9] The convergence improves if the sum in (3.11) is averaged over a few successive levels. Figure 13 shows the singularity spectrum determined using the periodic points of period 9–13. It is worthwhile to mention that $\alpha_{\max}$ and $\alpha_{\min}$ are determined by the fixed point and the period 2, respectively.

C. Metric properties of the Hénon attractor

The Hénon map is not hyperbolic. We might therefore expect marginal orbit points that exist near turnbacks to have some role in determining the metric properties. We first found all the orbits of the Hénon map with $a=1.4, b=0.3$, up to length 21. Using Eqs. (3.16)–(3.17), we solved for α_1 and α_2 using eigenvalues of orbits with n-$2n$ being 6-12, 7-14, 8-16, 9-18, and 10-20. The picture that emerges is the following: in almost all the boxes $\alpha_1=1$. Very rarely, we find orbits of length $2n$ whose eigenvalues $\lambda_1^{(2n)}$ are much smaller than $O(2\lambda_1^{(n)})$. This occurs twice in the 8-16 data set, and three times in the 10-20 data set. The value of α in all these cases comes to $\alpha\approx 0.72$ with $\alpha_1\approx 0.59$. These isolated events are to be compared with thousands of boxes in which $\alpha_1=1$. The meaning of this is that even the Hénon attractor is almost everywhere hyperbolic, and the nonhyperbolicity is a delicate phenomenon.

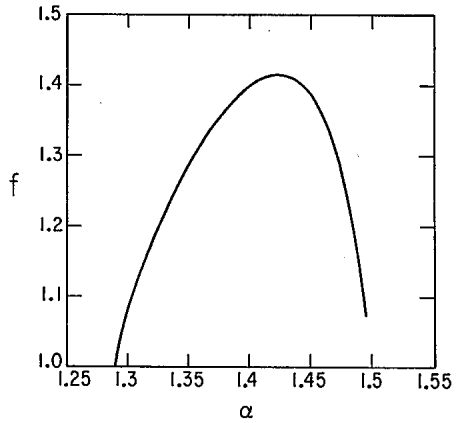

FIG. 13. $f(\alpha)$ for the Lozi map with $a=1.7, b=0.5$.

The limited amount of data leaves the following possibilities open.

(i) The isolated α values, $\alpha<1$, are found on a set of zero Hausdorff measure, or $f=0$.

(ii) The isolated α values are to be found on all the turnbacks, and are therefore associated with a set of dimension comparable to the transverse Cantor dimension (~ 0.27 for these parameter values).

(iii) Every turnback contributes a somewhat different $\alpha<1$, each of which is associated with $f=0$.

The limited information at hand indicates that the num-

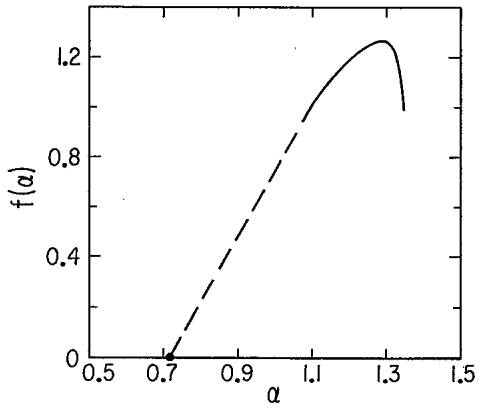

FIG. 14. $f(\alpha)$ for the Hénon map with $a=1.4, b=0.3$. There is an apparent phase transition which is linked to the nonhyperbolic nature of this map, and is believed to be generic.

ber of events in which $\alpha<1$ is not growing exponentially with n. We thus feel inclined to believe the first possibility (i), but further work to substantiate this feeling is needfurther work to substantiate this feeling is needed.

From the global point of view we can calculate $\tau(q)$ from Eq. (3.6) as explained above. Legendre transforming, we obtain the solid line of the $f(\alpha)$ curve shown in Fig. 14. The numerics asymptote to $\alpha=1$ already between $q=2.2$ and $q=2.4$. The global calculation fails to reach the isolated α values obtained by the local analysis, because of their extreme rarity. Adding the value $\alpha\approx.72$ onto the $f=0$ axis, we see, however, that a straight line of slope 2.3 connects well onto the solid curve calculated by the global approach. Since a straight portion in the $f(\alpha)$ curve translates to a nonanalyticity in the q dependence of $\tau(q)$, this phenomenon can be interpreted as a phase transition in the thermodynamic interpretation of the multifractal properties. Such an interpretation is in agreement with a recent conjecture by Grassberger, Badii, and Politi.[33]

IV. CONCLUSIONS

We have shown that the set of all allowed periodic orbits in Hénon-type maps can be understood theoretically. The allowed and disallowed orbits are separated in the symbol plane by the pruning front, and the latter can be obtained systematically at well-chosen points in parameter space, using the fact that its discontinuities are ordered by $O(b^n)$. Low-order calculations were done explicitly showing that Hénon-type maps have practically universal topologies to the order considered. Thus, although in principle there is no finite-codimension universality, in practice, for b small enough, the control of two parameters yields universal distributions of periodic orbits for orbits which are not too long. Next we have shown that the ergodic and metric properties of the strange attractors can be systematically calculated by organizing them about the periodic orbits. Calculations for Lozi and Hénon maps indicate the essential metric differences between hyperbolic and nonhyperbolic systems. The latter exhibit apparent phase transitions in their multifractal properties.

The application of these ideas to quantitative analysis of experimental data sets remains for future work. Of particular interest is the question of whether the organization about periodic orbits might help in predicting the future evolution of chaotic deterministic systems.

ACKNOWLEDGMENTS

This work has been supported in part by the Office of Naval Research under Grant No. N00014-84-K-0312 and by the Department of Energy under Grant No. DE-AC02-83ER13044. A part of this work was done at the Aspen Center for Physics Workshop on Chaos. P. C. thanks the Laboratory of Atomic and Solid Physics, Cornell University for their hospitality. I. P. acknowledges partial support by the U.S.–Israel Binational Science Foundation and by the Minerva Foundation, Munich, Germany. We are grateful to M. J. Feigenbaum for his contributions to this project. Conversations with J. Guckenheimer, P. J. Holmes, L. P. Kadanoff, and C. Tresser are much appreciated.

APPENDIX A

The order (on the axis) of two points x and y can be determined from their itineraries $\{a_k\}$ and $\{b_k\}$ as follows.[12,19] Suppose $a_1=b_1,\ldots,a_k=b_k$ and $a_{k+1}=0$ and $b_{k+1}=1$. Then

$$x<y \Longleftrightarrow \sum_{i=1}^{k} a_i(\mathrm{mod}2)=0 \ . \tag{A1}$$

To prove this, first note that if $a_1=0$ and $b_1=1$, then x and y are, respectively, to the left and the right of the critical point and hence $x<y$. Next suppose that $a_1=b_1$, $a_2=0$, and $b_2=1$. The latter two conditions imply that $f(x)<f(y)$, and hence that

$$f'(z)(x-y)<0 \tag{A2}$$

for some $z\in(x,y)$. But $f'(z)$ is positive or negative according to as $a_1=0$ or 1, and the result follows. Next suppose that the first k symbols are equal. Then from $a_{k+1}=0$ and $b_{k+1}=1$, it follows that

$$f^{(k)}(x)<f^{(k)}(y) \ . \tag{A3}$$

Since the first k symbols of the itineraries are identical,

$$f^{(k)}(x)-f^{(k)}(y)=f'[f^{(k-1)}(z)] \times f'[f^{(k-2)}(z)]\ldots f'(z)(x-y) \ , \tag{A4}$$

where $z\in(x,y)$. Hence

$$x<y \Longleftrightarrow f'[f^{(k-1)}(z)]f'[f^{(k-2)}(z)]\ldots f'(z)>0 \ . \tag{A5}$$

By (2.1), $f'[f^{(i)}(x)]>0 \Longleftrightarrow a_{i+1}=0$, and (2.3) follows.

APPENDIX B

We will determine the structure of the symbol plane for the Lozi attractor at the crisis point. First we observe that the tangent bifurcations will occur when a point of the periodic orbit crosses the y axis, and then, expanding to linear order about the tent map, determine which orbits will be disallowed.

We rewrite the Lozi map as

$$\begin{aligned} x' &= y+(a-1)+\eta a x \ , \\ y' &= bx \ , \end{aligned} \tag{B1}$$

where $\eta=-\mathrm{sgn}x$. The crisis for the Lozi attractor occurs at $a=(2-1/2b)$ (Ref. 22). The outer edges of the Lozi attractor are shown in Fig. 15. The coordinates of the points marked are

$$\begin{aligned} &x_0=\tfrac{1}{3}, \quad y_0=\tfrac{1}{3}b \ , \\ &x_A=0, \quad y_A=\tfrac{1}{2}b \ , \\ &x_B=1, \quad y_B=0 \ . \end{aligned} \tag{B2}$$

As b increases, the coordinates of a given periodic point

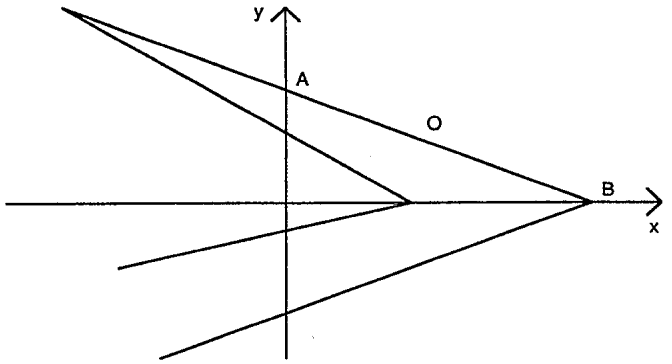

FIG. 15. The outer edge of the Lozi attractor (see Appendix B).

will vary smoothly. Hence in order for a tangent bifurcation to occur, some point of the orbit will have to cross the y axis. Thus an inverse tangent bifurcation (which will make the corresponding orbit disallowed) will also occur when a point in the orbit crosses the y axis.

The tent map

$$x'=1+2\eta x \tag{B3}$$

is Smale complete, and contains a unique periodic point corresponding to any symbol sequence. We need to find out which of these orbits will be disallowed as b increases from zero. Consider an orbit $(x_1^{(0)},x_2^{(0)},\ldots,x_N^{(0)})$ of the tent map and assume that $x_k^{(0)}$ is the point that will cross the y axis to cause the inverse tangent bifurcation. Since $x_k^{(0)}$ is close to the origin, we write it as

$$x_k^{(0)}=-\epsilon\eta_k \ , \tag{B4}$$

where $\epsilon \ll 1$. The points that have the potential of crossing the y axis have to be within a distance ϵ_0 (to the axis) which is linear in b. Hence we rewrite (A4) as

$$x_k^{(0)}=-bs\eta_k \ , \tag{B5}$$

where $s\sim 1$. Its image and preimage are

$$\begin{aligned} x_{k+1}^{(0)}&=1-2bs \ , \\ x_{k-1}^{(0)}&=-\tfrac{1}{2}(\eta_{k-1}+bs\eta_k\eta_{k-1}) \ . \end{aligned} \tag{B6}$$

For small b we write the corresponding orbit of the Lozi attractor as $(x_1,x_2,\ldots,x_N)$. The expanding in linear order in b

$$x_m=x_m^{(0)}+bt_m, \quad m=1,2,\ldots,N \ . \tag{B7}$$

From (A1) to linear order in b,

$$\begin{aligned} x_{x+1}^{(0)}+bt_{k+1}=bx_{k-1}^{(0)}&+(1-\tfrac{1}{2}b) \\ &+\eta_k(2-\tfrac{1}{2}b)(-bs\eta_k+bt_k) \end{aligned} \tag{B8}$$

at crisis. The analogous equation for the tent map is

$$x_{k+1}^{(0)}=1-2bs \ . \tag{B9}$$

Subtracting (A9) from (A8) gives

$$t_{k+1}=-\tfrac{1}{2}(\eta_{k-1}+1)+2\eta_k t_k \ . \tag{B10}$$

Now suppose $\eta_{k-1}=-1$. Then (A10) reduces to

$$t_{k+1}=2\eta_k t_k \ . \tag{B11}$$

But for (x_k,y_k) to cross the y axis,

$$0=x_k=x_k^{(0)}+bt_k\rightarrow t_k=s\eta_k \ . \tag{B12}$$

Hence

$$t_{k+1}=2s \ ,$$

and so

$$x_{k+1}=x_{k+1}^{(0)}+bt_{k+1}=1 \ . \tag{B13}$$

Hence (x_{k+1},y_{k+1}) is the point B. But all preimages of B are on AB, and so it cannot be a periodic point. Thus $\eta_{k-1}=-1$, which is what we needed to prove.

[1]M. Hénon, Commun. Math. Phys. **50**, 69 (1976).
[2]D. Ruelle and J.-P. Eckmann, Rev. Mod. Phys. **57**, 617 (1985).
[3]P. Cvitanovic, *Universality in Chaos* (Hilger, Bristol, 1984).
[4]U. Bali-Lin Hao, *Chaos* (World Scientific, Singapore, 1984).
[5]E. N. Lorenz, J. Atmos. Sci. **20**, 130 (1963).
[6]T. C. Halsey, N. H. Jensen, L. P. Kadanoff, I. Procaccia, and B. I. Shraiman, Phys. Rev. A **33**, 1141 (1986).
[7]D. Ruelle and F. Takens, Commun. Math. Phys. **20**, 167 (1971).
[8]D. Auerbach, P. Cvitanovic, J.-P. Eckmann, G. H. Gunaratne, and I. Procaccia, Phys. Rev. Lett. **58**, 2387 (1987).
[9]D. Auerbach, B. O'Shaughnessy, and I. Procaccia, Phys. Rev. A **37**, 2234 (1988).
[10]G. H. Gunaratne and I. Procaccia, Phys. Rev. Lett. **59**, 1377 (1987).
[11]R. Lozi, J. Phys. (Paris) Colloq. **39**, C5–9 (1978).
[12]P. J. Myrberg, Ann. Acad. Sci. Fenn., Ser. A **259**, 1 (1958).
[13]D. Fournier, H. Kawakami, and C. Mira, C. R. Acad. Sci., Ser. A **298**, 253 (1984); **301**, 325 (1985); **301**, 223 (1985).
[14]O. Chavoya-Aceues, F. Angulo-Brown, and E. Pina, Physica **14D**, 374 (1985).
[15]G. H. Gunaratne, M. H. Jensen, and I. Procaccia, Nonlinearity **1**, 157 (1988).
[16]We stress that this set is not always seen in an experiment. Only when *all* the periodic orbits are unstable is this the skeleton of the observed set.
[17]The fact that we are able to systematically construct the union of all periodic points and compute its Hausdorff dimension and the scaling spectrum does not establish the existence of the strange attractors; it merely establishes an upper bound on its dimension.
[18]N. Metropolis, M. L. Stein, and P. R. Stein, J, Comb. Theor. A **15**, 25 (1973).
[19]P. Collet and J.-P. Eckmann, *Iterated Maps on the Interval as Dynamical Systems* (Birkhauser, Boston, 1980).

[20]J. Guckenheimer and P. J. Holmes, *Nonlinear Oscillations, Dynamical Systems and Bifurcations of Vertex Fields* (Springer, New York, 1983).
[21]S. Simo, J. Stat. Phys. **21**, 21 (1979).
[22]S. Smale, Bull. Am. Math. Soc. **73**, 747 (1967).
[23]P. Grassberger and H. Kantz, Phys. Lett. A **113**, 235 (1985).
[24]M. Misiurewicz, Ann. Acad. Sci. (N.Y.) **357**, 348 (1972).
[25]Ç. Grebogi, E. Ott, and J. A. Yorke, Phys. Rev. Lett. **48**, 1507 (1982).
[26]T. Tel, Z. Phys. B **49**, 157 (1982); Phys. Lett. **94A**, 334 (1983); J. Stat. Phys. **33**, 195 (1983).
[27]M. J. Feigenbaum, M. H. Jensen, and I. Procaccia, Phys. Rev. Lett. **57**, 1503 (1986); M. H. Jensen, L. P. Kadanoff, and I. Procaccia, Phys. Rev. A **36**, 1409 (1987).
[28]H. Hata, thesis, Kyushu University, Fukuoka, Japan, 1987.
[29]D. Katzen and I. Procaccia, Phys. Rev. Lett. **58**, 1169 (1987).
[30]P. Cvitanovic, in *XV International Colloquium on Group Theoretical Methods in Physics,* edited by R. Gilmore (World Scientific, Singapore, 1987).
[31]S. Newhouse, Publ. Math. IHES **50**, 101 (1980).
[32]I. Procaccia, Nucl. Phys. B (to be published).
[33]P. Grassberger, R. Badii, and A. Politi (unpublished).